# A Locally Conformed Finite-Difference Time-Domain Algorithm of Modeling Arbitrary Shape Planar Metal Strips

Jiayuan Fang, *Member, IEEE,* and Jishi Ren

***Abstract*—A general algorithm to model arbitrary shape planar metal strips by the finite-difference time-domain (FDTD) method is presented in this paper. With this method, fields in the entire computation domain are computed by the regular FDTD algorithm except those near metal strips where special techniques proposed in this paper are applied. Unlike globally conformed finite-difference algorithms, the computation efficiency of the regular FDTD method is maintained while high space-resolution is obtained by this locally conformed finite-difference method. Numerical tests have verified that a higher computation accuracy is achieved by this scheme than the conventionally used staircase approximation. The modeling of electrical characteristics of two crossed strip lines is provided as an example.**

## I. Introduction

THE finite-difference time-domain method has been applied to many electromagnetic problems in antennas, scattering and microwave circuit components [1]–[3]. In dealing with complex shape objects, where the boundaries of objects do not coincide with finite-difference grid lines, the staircase approximation is commonly used [3]. Due to the low space resolution of the staircase approximation, a very fine mesh has to be used to accurately represent object geometries, which can easily result in an excessive requirement of computer resources.

To overcome the difficulties in the staircase approximation, finite-difference algorithms in nonorthogonal coordinates have been proposed and applied to various problems [4]–[6]. With nonorthogonal finite-difference algorithms, finite-difference grids are conformed to surfaces of modeled objects in the way similar to that in finite-element methods. Although the resolution of surfaces of objects is significantly improved, nonorthogonal finite-difference algorithms usually require much longer computation times than the regular FDTD algorithm for the same size of problems [6]. It is also very challenging to generate grids in nonorthogonal coordinates for three-dimensional complex shape objects.

Manuscript received May 19, 1992; revised September 25, 1992. This work was supported by the National Science Foundation under contract MIP-9110203 and ECD-9108850 which supports the Integrated Electronics Engineering Center (IEEC) at the State University of New York at Binghamton.

J. Fang is with the Department of Electrical Engineering, State University of New York at Binghamton, Binghamton, NY 13902.

J. Ren was a visiting scholar at the Department of Electrical Engineering, State University of New York at Binghamton, from the Department of Electrical Engineering Northwestern Polytechnical University, Xi'an 710072, P. R. of China.

IEEE Log Number 9207412.

To maintain the computation efficiency of the original FDTD method, instead of globally deforming the grid as in nonorthogonal finite-difference algorithms, we propose a locally conformed finite-difference algorithm for modeling arbitrary shape planar metal strips. With this method, fields in the whole computation domain are first computed by the regular FDTD algorithm, fields near metal strips are then corrected according to locations of metal edges in the finite-difference mesh. The additional computation required in the present method to correct fields near irregular shape objects is only a small percentage of the overall computation still dominated by the regular FDTD operations, while the same improvement on the space-resolution is achieved by this method as by the nonorthogonal finite-difference algorithms. It will be shown that the numerical error, such as the artificially slowed propagation speed in the staircase approximation [7], can be substantially reduced by the present method.

The main idea of the locally conformed finite-difference method presented in this paper is based on the integral form of Maxwell's equations. This approach has been applied to model curved surfaces in two dimensional problems [8], and conducting wires and strips which are parallel to finite-difference grid lines in three dimensional problems [9]. In this paper we will present a method of properly applying the integral form of Maxwell's equations for modeling arbitrary shape planar metal strips in three dimensional problems.

## II. Locally Conformed Finite- Difference Algorithm

The finite-difference time-domain method proposed by K. S. Yee [1] is based on the discretization of Maxwell's curl equations by the central-difference approximation in both space and time. With given initial and boundary conditions, the electric and magnetic field components are computed alternatively in the leap-frog manner for some known source excitations. When edges of metal strips are approximated by stair-stepped boundaries, all field components are computed by the regular FDTD algorithm except that the tangential electric and normal magnetic field components on metal surfaces are set to zero.

The general procedure of computation by our locally conformed finite-difference algorithm consists of the following steps for problems involving metal strips:

1. Calculate the electric field at time-step $n$ in the entire computation domain by the regular FDTD algorithm.
2. Set tangential electric field components at time-step $n$ to zero on surfaces of metal strips.

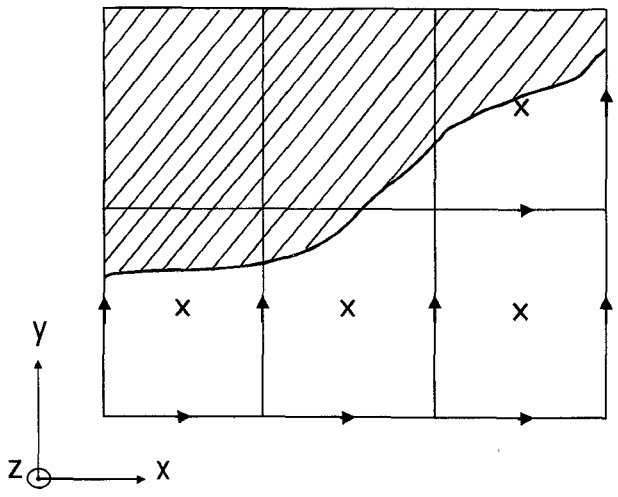


Fig. 1. Metal strip on a finite-difference mesh. $\times H_z$ nodes; $\rightarrow E_x$ nodes; $\uparrow E_y$ nodes.

3. Calculate the magnetic field at time-step $n + 1/2$ in the entire computation domain by the regular FDTD algorithm.
4. Set normal magnetic field components at time-step $n + 1/2$ to zero on surfaces of metal strips.
5. Correct the electric field components at time-step $n$, and the magnetic field components at time-step $n + 1/2$ around metal strips that can not be found by the regular FDTD algorithm.

Steps 1 to 4 above are straightforward regular FDTD computations. What needs to be explained is step 5 on the correction of electric and magnetic fields near metal strips.

As shown in Fig. 1, suppose a metal strip of zero thickness is placed on the $x$-$y$ plane. The edge of the metal strip can pass across the finite-difference mesh in many different ways, resulting in different types of irregular elements near the metal strip. Different types of elements may require different correction procedures. When the angle between the edge of the metal strip and the $x$ axis is between 0° to 45°, all possible cases of irregular elements are listed in Fig. 2 according to positions of various field components near the metal strip. It is generally sufficient to consider the computation of field components for cases listed in Fig. 2 only. In case the angle between the metal edge and the $x$ axis is larger than 45°, the angle between the metal edge and the $y$ axis is then less than 45°, and therefore the technique of dealing with elements in Fig. 2 can be applied accordingly by replacing the $x$ axis in Fig. 2 by the $y$ axis.

For elements near metal strips listed in Fig. 2, field components $H_z, E_y, E_x, H_y$ and $H_x$ need to be computed specially when they can not be computed by the regular FDTD algorithm. The sixteen types of elements in Fig. 2 can be categorized to five groups, as listed in Table I, according to their corresponding correction procedures of field components. Next, we will discuss procedures of correcting field components near metal strips for each group of elements.

*Group A:* The field components associated with this element, which is redrawn in Fig. 3, that can not be found by the regular FDTD algorithm are $H_z(i,j,k), H_x(i,j,k)$ and

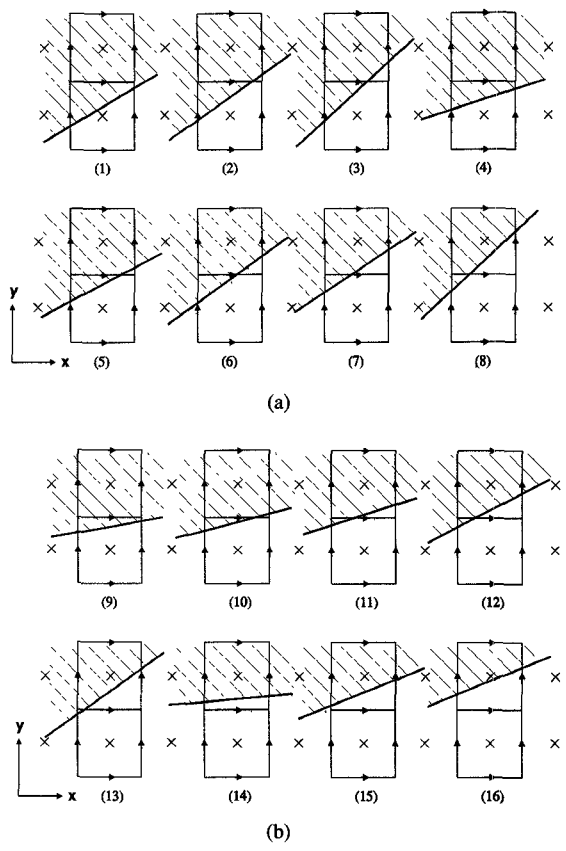


Fig. 2. (a) Finite-difference elements near metal strips. $\times H_z$ nodes; $\rightarrow E_x$ nodes; $\uparrow E_y$ nodes. (b) Finite-difference elements near metal strips. $\times H_z$ nodes; $\rightarrow E_x$ nodes; $\uparrow E_y$ nodes.

TABLE I
CATEGORIZATION OF IRREGULAR ELEMENTS LISTED IN FIG. 2

| | Group A | Group B | Group C | Group D | Group E |
|---|---|---|---|---|---|
| Elements in Figure 2 | (9) | (10),(11), (12),(13) | (14),(15), (16) | (1),(4) | (2),(3),(5), (6),(7),(8) |

$H_x(i,j,k-1)$. $H_x(i,j,k)$ is located half space-step above $E_y(i,j,k)$ in the $z$ direction, and $H_x(i,j,k-1)$ is located half space-step below $E_y(i,j,k)$ in the $z$ direction. The correction procedure consists of following processes:

(a) Correcting $H_z^{n+1/2}(i,j,k)$.

From Faraday's law,

$$\oint_{c_1} \vec{E} \cdot d\vec{l} = -\mu \frac{\partial}{\partial t} \int_{s_1} \vec{H} \cdot d\vec{S}, \tag{1}$$

where $c_1$ is the loop ABCDA shown in Fig. 3, and $s_1$ is the area enclosed by loop $c_1$. Discretizing (1) results in the following difference equation for computing $H_z(i,j,k)$ at time-step $n + 1/2$.

$$\begin{aligned} H_z^{n+1/2}(i,j,k) = H_z^{n-1/2}(i,j,k) - \frac{dt}{\mu s_1} \\ \cdot [-E_y^n(i,j,k) \cdot l_{\mathrm{AB}} + E_x^n(i,j,k) \\ \cdot dh + E_y^n(i+1,j,k) \cdot l_{\mathrm{CD}}] \end{aligned} \tag{2}$$

where $dt$ is the time-step, $dh$ is the space-step of the finite-difference grid, $l_{\mathrm{AB}}$ and $l_{\mathrm{CD}}$ are the lengths of sides AB and

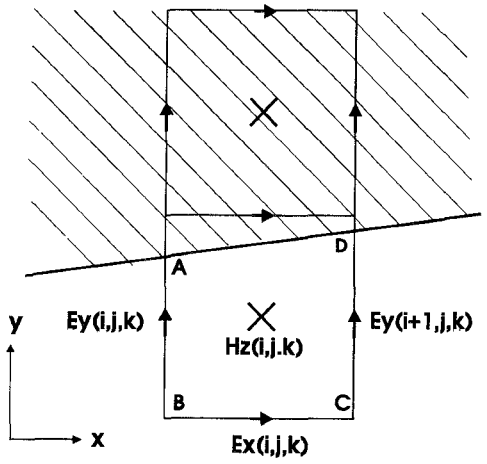


Fig. 3. An element of group $A$.

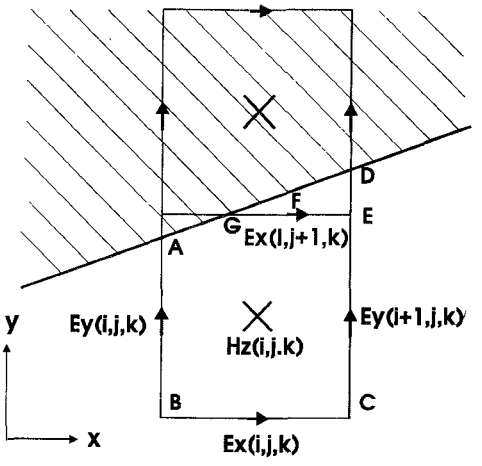


Fig. 4. An element of group $B$.

CD. The electric field component along the metal edge is assumed to be zero.

(b) Correcting $H_x^{n+1/2}(i,j,k)$ and $H_x^{n+1/2}(i,j,k-1)$.

The finite-difference algorithms for computing $H_x^{n+1/2}(i,j,k)$ and $H_x^{n+1/2}(i,j,k-1)$ need to be modified from the regular FDTD algorithms by taking into account that $E_y^n(i,j,k)$ is nonzero only across the length $l_{\mathrm{AB}}$. The modified difference equations for computing $H_x^{n+1/2}(i,j,k)$ and $H_x^{n+1/2}(i,j,k-1)$ are:

$$\begin{aligned} H_x^{n+1/2}(i,j,k) &= H_x^{n-1/2}(i,j,k) - \frac{dt}{\mu\cdot dh}\Big[E_y^n(i,j,k)\cdot\frac{l_{\mathrm{AB}}}{dh} \\ &\quad + E_z^n(i,j+1,k) - E_y^n(i,j,k+1) - E_z^n(i,j,k)\Big], \quad (3) \end{aligned}$$

$$\begin{aligned} H_x^{n+1/2}(i,j,k-1) &= H_x^{n-1/2}(i,j,k-1) - \frac{dt}{\mu\cdot dh}\Big[E_y^n(i,j,k-1) \\ &\quad + E_z^n(i,j+1,k-1) - E_y^n(i,j,k)\cdot\frac{l_{\mathrm{AB}}}{dh} \\ &\quad - E_z^n(i,j,k-1)\Big]. \quad (4) \end{aligned}$$

In the term $l_{\mathrm{AB}}/dh = 1$, (3) and (4) will become the regular FDTD equations for computing $H_x^{n+1/2}(i,j,k)$ and $H_x^{n+1/2}(i,j,k-1)$. In dealing with the element in Fig. 3, there is no need to correct $H_x^{n+1/2}(i+1,j,k)$ and $H_x^{n+1/2}(i+1,j,k-1)$ located half space-step above and below $E_y(i+1,j,k)$ in the $z$ direction, because these components will be taken care of when the neighboring element at the right is being processed.

*Group B:* A typical element of this group is drawn in Fig. 4. The field components need to be corrected are $H_z(i,j,k), E_x(i,j+1,k), H_y(i,j+1,k), H_y(i,j+1,k-1), H_x(i,j,k)$ and $H_x(i,j,k-1)$. $H_y(i,j+1,k)$ is located half space-step above $E_x(i,j+1,k)$ in the $z$ direction, and $H_y(i,j+1,k-1)$ is located half space-step below $E_x(i,j+1,k)$ in the $z$ direction. The correction procedure of this group of elements is described below:

(a) Correcting $H_z^{n+1/2}(i,j,k)$.

$H_z^{n+1/2}(i,j,k)$ is computed in the same way as that for group $A$ elements. Faraday's law is applied along the loop ABCDA denoted in Fig. 4, resulting in (2) for computing $H_z^{n+1/2}(i,j,k)$.

(b) Correcting $E_x^n(i,j+1,k)$.

The location of the node of $E_x(i,j+1,k)$ is assumed to be at the point F in Fig. 4, which is at the middle of the side EG. $E_x^n(i,j+1,k)$ is calculated by making use of the corrected value of $H_z^{n+1/2}(i,j,k)$ obtained in process (a) above. From Faraday's law expressed in (1), replacing $c_1$ and $s_1$ in (1) by $c_2$ and $s_2$, where $c_2$ is the loop ABCEFGA and $s_2$ is the area enclosed by loop $c_2$, the difference equation for correcting $E_x^n(i,j+1,k)$ is obtained as

$$\begin{aligned} E_x^n(i,j+1,k) &= \frac{1}{l_{\mathrm{EG}}}[E_x^n(i,j,k)\cdot dh + E_y^n(i+1,j,k)\cdot dh \\ &\quad - E_y^n(i,j,k)\cdot l_{\mathrm{AB}}] + \frac{\mu s_2}{dt\cdot l_{\mathrm{EG}}}[H_z^{n+1/2}(i,j,k) \\ &\quad - H_z^{n-1/2}(i,j,k)]. \quad (5) \end{aligned}$$

(c) Correcting $H_y^{n+1/2}(i,j+1,k)$ and $H_y^{n+1/2}(i,j+1,k-1)$

With the newly corrected $E_x^n(i,j+1,k)$ in process (b), $H_y^{n+1/2}(i,j+1,k)$ and $H_y^{n+1/2}(i,j+1,k-1)$ are computed by the modified FDTD algorithms, that take into account that $E_x^n(i,j+1,k)$ is nonzero only across the length $l_{\mathrm{EG}}$. This is evident in equations (6) and (7), which are shown at the bottom of the next page.

(d) Correcting $H_x^{n+1/2}(i,j,k)$ and $H_x^{n+1/2}(i,j,k-1)$

$H_x^{n+1/2}(i,j,k)$ and $H_x^{n+1/2}(i,j,k-1)$ are computed in the same way as group $A$ elements by (3) and (4) respectively.

*Group C:* The field components need to be corrected for this group of elements are $H_z(i,j,k), E_x(i,j+1,k), H_y(i,j+1,k), H_y(i,j+1,k-1), H_x(i,j+1,k)$ and $H_x(i,j+1,k-1)$. A typical element of this group is drawn in Fig. 5. The correction procedure of this group of elements is:

(a) Correcting $H_z^{n+1/2}(i,j,k)$ by (2) where $s_1$ is the area enclosed by the loop $ABCDA$.

(b) Correcting $E_x^n(i,j+1,k)$. $E_x^n(i,j+1,k)$ is computed in the same way as that for group $B$ elements, except that

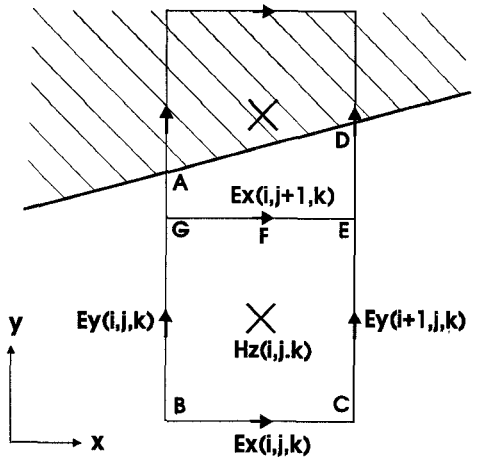


Fig. 5. An element of group $C$.

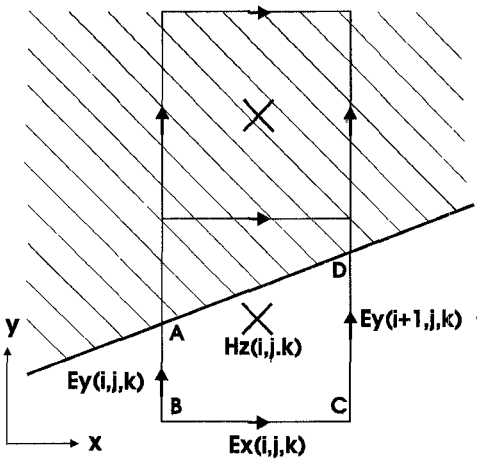


Fig. 6. An element of group $D$.

the loop $c_2$ (GBCEFG) encloses a rectangle formed by finite-difference grid lines. The difference equation for correcting $E_x^n(i, j+1, k)$ is therefore:

$$\begin{aligned} & E_x^n(i,j+1,k) \\ &= E_x^n(i,j,k) + E_y^n(i+1,j,k) - E_y^n(i,j,k) \\ &\quad + \frac{\mu \cdot dh}{dt}[H_z^{n+1/2}(i,j,k) - H_z^{n-1/2}(i,j,k)]. \end{aligned} \tag{8}$$

(c) Correcting $H_y^{n+1/2}(i, j+1, k)$ and $H_y^{n+1/2}(i, j+1, k-1)$.

$H_y^{n+1/2}(i, j+1, k)$ and $H_y^{n+1/2}(i, j+1, k-1)$ are computed with the newly corrected $E_x^n(i, j+1, k)$ in process (b). Their difference equations are:

$$\begin{aligned} & H_y^{n+1/2}(i,j+1,k) \\ &= H_y^{n-1/2}(i,j+1,k) - \frac{dt}{\mu \cdot dh}[E_x^n(i,j+1,k+1) \\ &\quad - E_z^n(i+1,j+1,k) - E_x^n(i,j+1,k) \\ &\quad + E_z^n(i,j+1,k)], \end{aligned} \tag{9}$$

$$\begin{aligned} & H_y^{n+1/2}(i,j+1,k-1) \\ &= H_y^{n-1/2}(i,j+1,k-1) - \frac{dt}{\mu \cdot dh}[E_x^n(i,j+1,k) \\ &\quad - E_z^n(i+1,j+1,k-1) - E_x^n(i,j+1,k-1) \\ &\quad + E_z^n(i,j+1,k-1)]. \end{aligned} \tag{10}$$

(d) Correcting $H_x^{n+1/2}(i, j+1, k)$ and $H_x^{n+1/2}(i, j+1, k-1)$

The FDTD algorithms of computing $H_x^{n+1/2}(i, j+1, k)$ and $H_x^{n+1/2}(i, j+1, k-1)$ are modified by taking into account that $E_y$ is nonzero only along the side AG. Let the value of $E_y$ along side AG be approximated by $E_y(i, j, k)$, and stored at the node of $E_y(i, j+1, k)$. The difference equations for computing $H_x^{n+1/2}(i, j+1, k)$ and $H_x^{n+1/2}(i, j+1, k-1)$ become (11) and (12) at the bottom of the next page.

*Group D:* Consider a typical element of this group shown in Fig. 6. The procedure of computing field components, $H_z(i, j, k)$, $H_x(i, j+1, k)$ and $H_x(i, j+1, k-1)$, associated with this group of elements is explained as follows:

(a) Correcting $H_z^{n+1/2}(i, j, k)$.

$H_z^{n+1/2}(i, j, k)$ is computed by (2) where $E_y^n(i, j, k)$ represents $E_y$ along side AB in Fig. 6. $E_y^n(i, j, k)$ can not be obtained by the regular FDTD algorithm for this group of elements, and is approximated by $E_y^n(i, j-1, k)$.

(b) Correcting $H_x^{n+1/2}(i, j, k)$ and $H_x^{n+1/2}(i, j, k-1)$ by (3) and (4) respectively. Again, $E_y^n(i, j, k)$ in (3) and (4) is approximated by $E_y^n(i, j-1, k)$

*Group E:* Consider a typical element of this group shown in Fig. 7. The valuer of $E_y^n(i, j, k)$ located at the middle of side AB is approximated by that of $E_y^n(i, j-1, k)$. The procedure of correcting the rest of field components is:

(a) Correcting $H_z^{n+1/2}(i, j, k)$ by (2). (b) Correcting $E_x^n(i, j+1, k)$ by (5). (c) Correcting $H_y^{n+1/2}(i, j+1, k)$ and $H_y^{n+1/2}(i, j+1, k-1)$ by (6) and (7) respectively. (d) Correcting $H_x^{n+1/2}(i, j, k)$ and $H_x^{n+1/2}(i, j, k-1)$ by (3) and (4) respectively.

$$\begin{aligned} H_y^{n+1/2}(i,j+1,k) = H_y^{n-1/2}(i,j+1,k) - \frac{dt}{\mu \cdot dh}\Big[ & E_x^n(i,j+1,k+1) \\ & - E_z^n(i+1,j+1,k) - E_x^n(i,j+1,k) \cdot \frac{l_{\mathrm{EG}}}{dh} + E_z^n(i,j+1,k)\Big], \end{aligned} \tag{6}$$

$$\begin{aligned} H_y^{n+1/2}(i,j+1,k-1) = H_y^{n-1/2}(i,j+1,k-1) - \frac{dt}{\mu \cdot dh}\Big[ & E_x^n(i,j+1,k) \cdot \frac{l_{\mathrm{EG}}}{dh} \\ & - E_z^n(i+1,j+1,k-1) - E_x^n(i,j+1,k-1) + E_z^n(i,j+1,k-1)\Big]. \end{aligned} \tag{7}$$

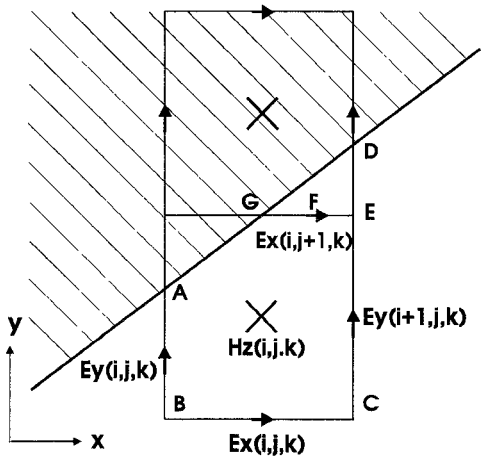


Fig. 7. An element of group $E$.

The procedures discussed above of correcting field components near metal strips for different groups of elements are summarized in Table II.

## III. Tests on the Locally Conformed Finite- Difference Algorithm

The locally conformed finite-difference algorithm, presented in the last section, can be tested by applying it to model a pulse propagation through a strip-line shown in Fig. 8. The strip line is oriented in an angle $\theta$ with the $x$ axis and surrounded by a dielectric medium of $\epsilon_r = 4$. The separation between two perfectly conducting reference planes is 1 mm. The metal strip is 0.4 mm above the lower reference plane. A uniform finite-difference mesh of equal space steps in the $x, y$ and $z$ directions is chosen for the computation. The space-step $dh$ is 0.2 mm, and the time-step $dt$ is 0.5 $dh$/v, where v is the speed of light in the medium. The width of the strip in the $y$ direction $W_y$ is chosen as 0.8 mm = 4 $dh$. The actual width of the strip is $W_y \cdot \cos\theta$.

Fig. 9 illustrates the staircase approximation of a strip line tilted from the $x$ axis by an angle $\theta = \tan^{-1}(1/3) = 18.4°$. It has been found that, due to the staircase approximation, a wave propagating along the conducting surface is artificially slowed down [7]. An alternative description of the numerical propagation speed along the strip line of Fig. 8 is the effective dielectric constant $\epsilon_{\text{reff}}$ which can be obtained from the transient solutions of fields along the strip line [2]. Suppose $u$ and $u+L$ are two positions separated by a distance $L$ along the strip line. $E(u,t)$ and $E(u+L,t)$ are numerically computed transient electric fields at the position $u$ and $u+L$. Denote the Fourier transforms of $E(u,t)$ and $E(u+L,t)$ as $E(u,\omega)$ and $E(u+L,\omega)$ respectively. For a wave propagating in the positive $u$ direction, $E(u,\omega)$ and $E(u+L,\omega)$ are related by

$$E(u+L,\omega) = E(u,\omega)e^{-\gamma(\omega)L}, \tag{13}$$

where

$$\gamma(\omega) = \alpha(\omega) + j\beta(\omega) \tag{14}$$

is the propagation constant. The effective dielectric constant $\epsilon_{\text{reff}}$ is defined as

$$\beta(\omega) = \omega\sqrt{\mu\epsilon_0\epsilon_{\text{reff}}}. \tag{15}$$

From (13) to (15), the effective dielectric constant $\epsilon_{\text{reff}}$ can be found from

$$\epsilon_{\text{reff}} = \frac{\beta^2}{\omega^2\mu\epsilon_0} = \frac{1}{\omega^2\mu\epsilon_0}\left[\frac{1}{L}\,\text{Imag}\left[\ln\left(\frac{E(u,\omega)}{E(u+L,\omega)}\right)\right]\right]^2 \tag{16}$$

where Image is the operator of taking the imaginary part of a complex number.

Since the strip line in Fig. 8 is surrounded by the uniform dielectric medium of $\epsilon_r = 4$, the effective dielectric constant $\epsilon_{\text{reff}}$ should be the same as $\epsilon_r$. However, the numerically computed effective dielectric constant $\epsilon_{\text{reff}}$ obtained by modeling a pulse propagation through a strip line is somewhat different from $\epsilon_r$, due to the computation error of the numerical scheme being used. The dashed curves in Fig. 10 are the computed effective dielectric constants of the strip line modeled by the staircase approximation for $\theta = 45°, 26.6°\,(= \tan^{-1}(1/2))$, $18.4°\,(= \tan^{-1}(1/3))$, $14.0°\,(= \tan^{-1}(1/4))$ and $11.3°\,(= \tan^{-1}(1/5))$. The reason for choosing these particular angles of $\theta$ is for the convenience of the staircase approximation of oblique strip lines as shown in Fig. 9. As can be seen from Fig. 10, $\epsilon_{\text{reff}}$'s obtained by the staircase approximation are all larger than the accurate solution of 4.0, representing slowed propagation speeds due to the numerical computation error, and the largest numerical error appears when $\theta = 45°$.

The effective dielectric constants of the strip line approximated by the locally conformed finite-difference algorithm of this paper are also shown in Fig. 10 by solid curves. It is seen that errors in the effective dielectric constants computed by the locally conformed finite-difference algorithm are about 60% to 70% smaller than those computed by the staircase approximation for the angles of $\theta$ chosen.

As a comparison, a locally conformed finite-difference algorithm based on a scheme in [8] is also tested. This scheme

$$H_x^{n+1/2}(i,j+1,k) = H_x^{n-1/2}(i,j+1,k) - \frac{dt}{\mu\cdot dh}[E_y^n(i,j+1,k)\cdot\frac{l_{\text{AG}}}{dh} + E_z^n(i,j+2,k) - E_y^n(i,j+1,k+1) - E_z^n(i,j+1,k)], \tag{11}$$

$$H_x^{n+1/2}(i,j+1,k-1) = H_x^{n-1/2}(i,j+1,k-1) - \frac{dt}{\mu\cdot dh}[E_y^n(i,j+1,k-1) + E_z^n(i,j+2,k-1) - E_y^n(i,j+1,k)\cdot\frac{l_{\text{AG}}}{dh} - E_z^n(i,j+1,k-1)]. \tag{12}$$

TABLE II
COMPUTATION OF FIELD COMPONENTS NEAR METAL STRIPS

| Field components to be corrected | Group A | Group B | Group C | Group D | Group E |
|---|---|---|---|---|---|
| $E_y^n(i,j,k)$ | — | — | — | $E_y^n(i,j-1,k)$ | $E_y^n(i,j-1,k)$ |
| $H_z^{n+1/2}(i,j,k)$ | equation (2) | equation (2) | equation (2) | equation (2) | equation (2) |
| $E_x^n(i,j+1,k)$ | — | equation (5) | equation (8) | — | equation (5) |
| $H_y^{n+1/2}(i,j+1,k)$ and $H_y^{n+1/2}(i,j+1,k-1)$ | — | equations (6) and (7) | equations (9) and (10) | — | equations (6) and (7) |
| $H_x^{n+1/2}(i,j,k)$ and $H_x^{n+1/2}(i,j,k-1)$ | equations (3) and (4) | equations (3) and (4) | — | equations (3) and (4) | equations (3) and (4) |
| $E_y^n(i,j+1,k)$ | — | — | $E_y^n(i,j,k)$ | — | — |
| $H_x^{n+1/2}(i,j+1,k)$ and $H_x^{n+1/2}(i,j+1,k-1)$ | — | — | equations (11) and (12) | — | — |

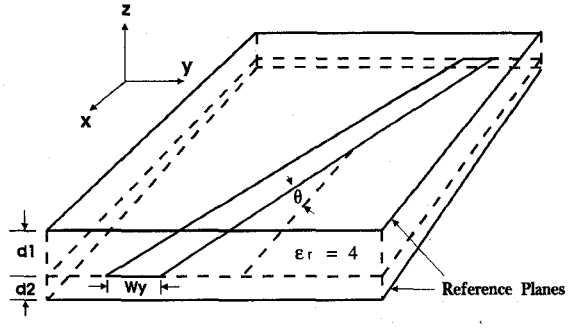


Fig. 8. Structure of a strip line tilted by an angle $\theta$ from the $x$ axis. $d1 = 0.6$ mm, $d2 = 0.4$ mm, $Wy = 0.8$ mm.

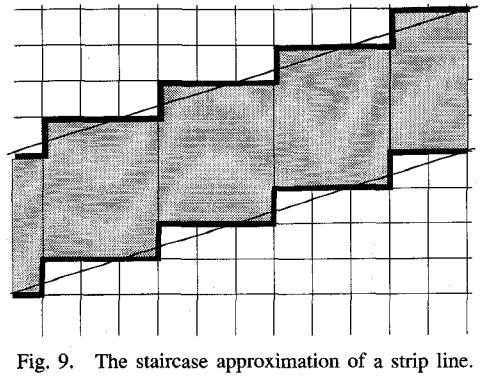

Fig. 9. The staircase approximation of a strip line.

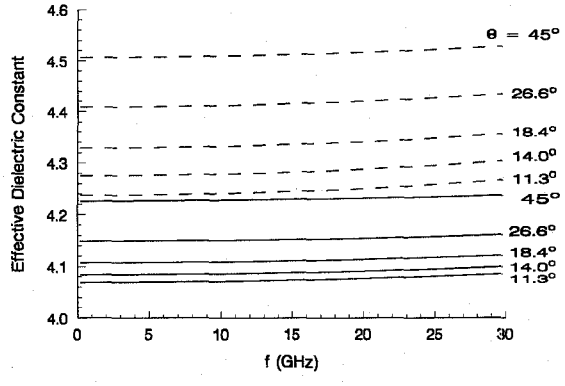


Fig. 10. Effective dielectric constants of a strip line computed by the staircase approximation (dashed curves) and the locally conformed finite-difference method of this paper (solid curves). The strip line is along the direction of an angle $\theta$ with the $x$ axis.

is called the "nearest neighbor approximation" in [8]. With this method applied to the strip line in Fig. 8, the irregular electric field components around the metal strip are approximated by their nearest neighbors of the same field components, and the irregular magnetic field components are calculated by applying the Faraday's law. The effective dielectric constant $\epsilon_{\text{reff}}(f)$ of the strip line computed by the "nearest neighbor approximation" are shown in Fig. 11 together with those obtained by the staircase approximation. It appears that an improvement on computation accuracy can also be made by the "nearest neighbor approximation," but not as much as that by the locally conformed finite-difference method of this paper.

## IV. NUMERICAL EXAMPLE

An example to illustrate the application of the locally conformed finite-difference algorithm for modeling microwave circuits is shown in Fig. 12. In this example, two strip lines are

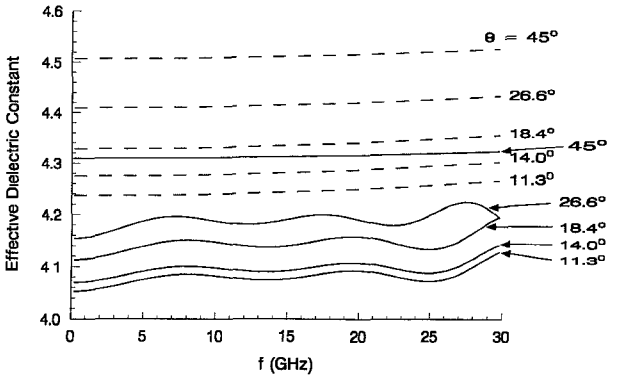


Fig. 11. Effective dielectric constants of a strip line computed by the staircase approximation (dashed curves) and the "nearest neighbor approximation" (solid curves). The strip line is along the direction of an angle $\theta$ with the $x$ axis.

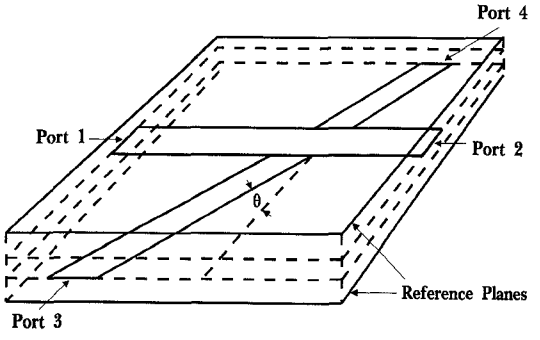


Fig. 12. Structure of two crossed strip lines.

crossed over each other with an angle $\theta$. The distance between two ground planes is 0.9 mm. Three layers of dielectrics between ground planes are all of thickness 0.3 mm and $\epsilon_r = 4$. The space-step $dh$ of the uniform finite-difference mesh is 0.1 mm. The time-step $dt$ is chosen as 0.5 $dh$/v. Both metal strips are of width $W = 0.4$ mm.

Apparently, for such structures as the ones shown in Fig. 12, the staircase approximation results in very poor resolutions of circuit geometries. By the application of the locally conformed finite-difference method, the numerical analysis of the dependence of the characteristics of the crossed strip lines on various parameters, such as the crossing angle $\theta$ and strip-line dimensions, becomes readily feasible.

The electrical properties of the two crossed strip lines are obtained by the numerical simulation of a pulse propagation through the structure. Let a Gaussian pulse propagate into the structure from port 1. The frequency dependent $S$ parameters of the structure are found by taking Fourier transforms of the reflected, transmitted and coupled waves. Fig. 13 shows the coupling coefficients $S_{13}$ and $S_{14}$ in the frequency range $f = 0$ to 15 GHz, as $\theta$ changes from 0° to 45° with a 5° interval. It is seen that, as expected, $S_{13}$ increases with increasing $\theta$, while $S_{14}$ decreases with increasing $\theta$. Both $S_{13}$ and $S_{14}$ increase with frequency in the frequency range of Fig. 13. An alternative presentation of $S_{13}$ and $S_{14}$ is shown in Fig. 14, where $S_{13}$ and $S_{14}$ at various frequencies are plotted as a

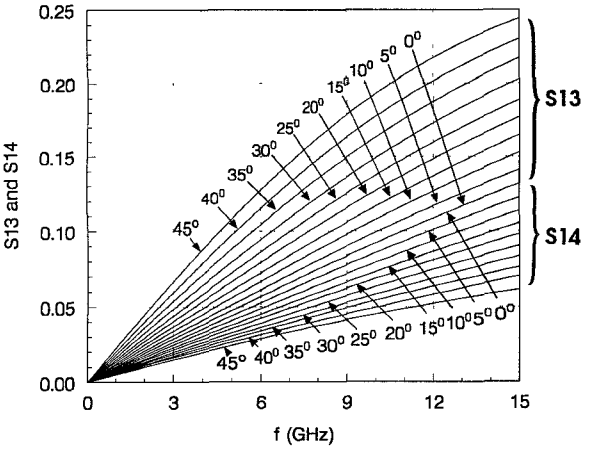


Fig. 13. Coupling coefficients between two crossed strip lines.

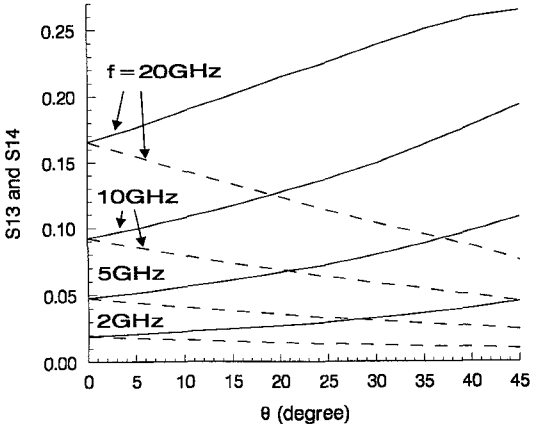


Fig. 14. Coupling coefficients ($S_{13}$ and $S_{14}$) between two crossed strip lines. Solid curves: $S_{13}$; Dashed curves: $S_{14}$.

function of the crossing angle $\theta$.

$S$ parameters obtained above can be post-processed to extract equivalent circuit parameters of the crossed strip-lines. For the equivalent circuit model consisted of capacitors $C_c, C_a$ and mutual inductor $M$ shown in Fig. 15, it can be derived that

$$MG_0 = \frac{S_{13} - S_{14}}{j2\pi f(1 - S_{11} + S_{12})}, \tag{17}$$

where $G_0$ is the characteristic admittance of the stip line, and

$$C_aZ_0 = \frac{1 - S_{11} - S_{12} - S_{13} - S_{14}}{j2\pi f(S_{12} + S_{14})(1 + j2\pi fMG_0)}, \tag{18}$$

$$C_cZ_0 = \frac{1 - S_{11} - S_{12} - j2\pi f(S_{12} + j2\pi fMG_0S_{14})C_aZ_0}{j2\pi f(S_{12} - S_{14})(1 - j2\pi fMG_0)}, \tag{19}$$

where $Z_0$ is the characteristic impedance of the strip line. Values of $C_cZ_0, C_aZ_0$ and $MG_0$ as a function of frequency for different crossing angles are displayed in Figs. 16, 17, and Fig. 18 respectively. The equivalent circuit model thus obtained can be used in computer-aided design tools to analyze crosstalk between strip lines with different terminations.

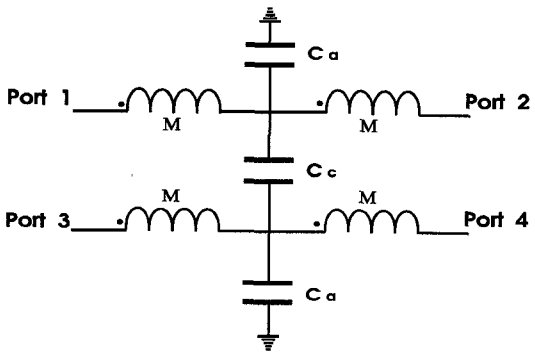


Fig. 15. The equivalent circuit of the crossed strip lines in Fig. 12.

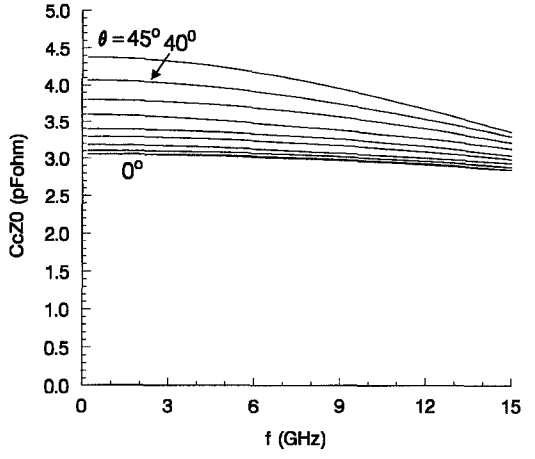


Fig. 16. Normalized equivalent capacitance $C_cZ_0$ of the crossed strip lines in Fig. 12 as a function of frequency. The crossing angle $\theta$ changes from 0° to 45° with 5° interval.

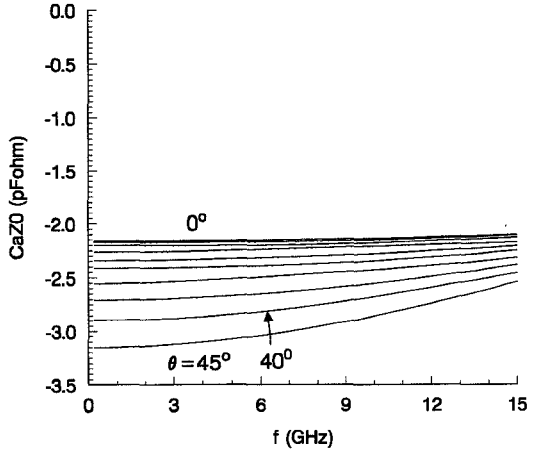


Fig. 17. Normalized equivalent capacitance $C_aZ_0$ of the crossed strip lines in Fig. 12 as a function of frequency. The crossing angle $\theta$ changes from 0° to 45° with 5° interval.

Strip-line crossings appear frequently in microwave circuits, but few results are available in present literatures on detailed analysis and modeling of strip-lines crossed with arbitrary angles. Although the computation results in Figs. 13–18 are believed to be highly reliable, they are subject to be compared with the results obtained by other numerical or experimental techniques.

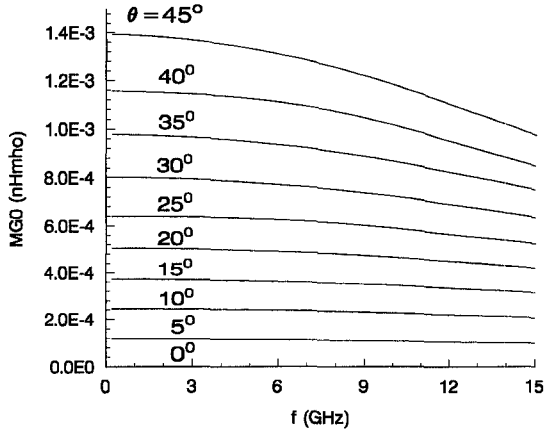


Fig. 18. Normalized equivalent inductance $MG_0$ of the crossed strip lines in Fig. 12 as a function of frequency. The crossing angle $\theta$ changes from 0° to 45° with 5° interval.

## V. Conclusion

A locally conformed finite-difference scheme is proposed in this paper to model arbitrary shape planar metal strips. This method is computationally more efficient than the globally conformed finite-difference schemes. Besides the high space-resolution of this method, it is also shown to be much more accurate than the staircase approximation. This method can be applied to various microwave planar circuits of complex shapes.

## References

[1] K. S. Yee, "Numerical solution of initial boundary value problems involving Maxwell's equations in isotropic media," *IEEE Trans. Antennas Propagat.*, vol. AP-14, pp. 302–307, May 1966.

[2] X. Zhang, J. Fang, K. K. Mei, and Y. Liu, "Calculation of the dispersive characteristics of microstrips by the time-domain finite-difference method," *IEEE Trans. Microwave Theory Tech.*, vol. 36, pp. 263–267, Feb. 1988.

[3] P. A. Tirkas and C. A. Balanis, "Finite-difference time-domain method for antenna radiation," *IEEE Trans. Antennas Propagat.*, vol. 40, pp. 334–340, Mar. 1992.

[4] R. Holland, "Finite-difference solution of Maxwell's equations in generalized nonorthogonal coordinates," *IEEE Trans. Nucl. Sci.*, vol. NS-30, pp. 4589–4591, Dec. 1983.

[5] M. A. Fusco, M. V. Smith, and L. W. Gordon, "A three-dimensional FDTD algorithm in curvilinear coordinates," *IEEE Trans. Antennas Propagat.*, vol. 39, pp. 1463–1471, Oct. 1991.

[6] J. F. Lee, R. Palandech, and R. Mittra, "Modeling three-dimensional discontinuities in waveguides using nonorthogonal FDTD algorithm," *IEEE Trans. Microwave Theory Tech.*, vol. 40, pp. 346–352, Feb. 1992.

[7] A. C. Cangellaris and D. B. Wright, "Analysis of the numerical error caused by the stair-stepped approximation of a conducting boundary in FDTD simulations of electromagnetic phenomena," *IEEE Trans. Antennas Propagat.*, vol. 39, pp. 1518–1525, Oct. 1991.

[8] T. G. Jurgens, A. Taflove, K. Umashankar, and T. G. Moore, "Finite-difference time-domain modeling of curved surfaces," *IEEE Trans. Antennas Propagat.*, vol. 40, pp. 357–366, Apr. 1992.

[9] A. Taflove, K. R. Umashankar, B. B. Beker, F. Harfoush, and K. S. Yee, "Detailed FDTD analysis of electromagnetic Fields penetrating narrow slots and lapped joints in thick conducting screens," *IEEE Trans. Antennas Propagat.*, vol. 36, pp. 247–257, Feb. 1988.

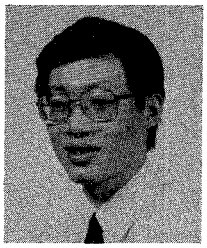

**Jiayuan Fang** (S'85–M'90) received the B.S.E.E. in electrical engineering in 1982 from Tsinghua University, Beijing, China, and the M.S. and Ph.D. degrees in electrical engineering from the University of California at Berkeley in 1987 and 1989 respectively.

Since 1990 he has been an assistant professor at the Department of Electrical Engineering, the State University of New York at Binghamton. He received the NSF Research Initiation Award in 1991, and the NSF Young Investigator Award in 1993. His research interests are numerical methods, electronic packaging, microwave circuit components modeling, antennas and scattering.

**Jishi Ren** was born in Shaanxi, China in 1953. He received his M.S. degree in electrical engineering from the Beijing Institute of Aeronautics and Astronautics in 1983. From 1983 to 1991, he taught in the Department of Electrical Engineering at Northwestern Polytechnical University (NPU) in China. At the same time, he studied microwave antennas, CAD of microwave circuits and electromagnetic scattering. Since 1990, he has been an Associate Professor in NPU. From July 1991 to June 1992, he worked on the modeling of integrated circuits as a visiting scholar in the State University of New York at Binghamton. Since July 1992, he has been a Research Associate at the Department of Electrical Engineering at the University of Utah. His current research focus is on the numerical computation of electromagnetic fields.

Mr. Ren was awarded the Research Prize by Chinese Aeronautics and Astronautics Ministry for his research work during the period of 1986 to 1990.